Development of Electrodeless Plasma Thrusters With High-Density Helicon Plasma Sources

Shunjiro Shinohara, Hiroyuki Nishida, Takao Tanikawa, Tohru Hada, Ikkoh Funaki, *Member, IEEE*, and Konstantin P. Shamrai (deceased)

Abstract—Helicon plasma sources are very useful in many aspects and are applicable to many fields across science and technology, as they can supply high-density ($\sim 10^{13}$ cm^{-3}) plasmas with a broad range of external operating parameters. In this paper, developed, featured sources with various sizes are characterized along with discussions on their particle production efficiency. This paper aims to develop systems that can realize schemes with completely electrodeless plasma production and acceleration. This is expected to mitigate the existing problems of the finite lifetimes inherent in electric plasma propulsion tools. Experimental and theoretical approaches that implement such schemes are presented.

Index Terms—Helicon wave, plasma production, plasma propulsion.

I. Introduction

HIGH-DENSITY, low temperature helicon plasmas (HPs) [1], [2] have been proven to be very effective for use in fundamental research as well as in a variety of additional applications. This is because the helicon sources can produce high-density ($\sim 10^{13}$ cm^{-3}) plasmas with a broad range of external operating parameters such as the fill pressure, the magnetic field strength and its field configuration as long as the excitation frequency is between the ion and electron cyclotron frequencies. Therefore, further development on the extension of the helicon source dimensions along with detailed characterization, is important for potential future applications. In this paper, various sizes of high-density (up to 10^{13} cm^{-3}) helicon sources [3]–[5] are developed with a very wide range of diameters between 0.5 and 74 cm. The discharge performance and wave characteristics are examined, bearing in mind the

S. Shinohara and H. Nishida are with the Institute of Engineering, Tokyo University of Agriculture and Technology, Tokyo 184-8588, Japan (e-mail: sshinoha@cc.tuat.ac.jp; hnishida@cc.tuat.ac.jp).

T. Tanikawa is with the Research Institute of Science and Technology, Tokai University, Kanagawa 259-1292, Japan (e-mail: tnth@keyaki.cc.u-tokai.ac.jp).

T. Hada is with the Interdisciplinary Graduate School of Engineering Sciences, Kyushu University, Fukuoka 816-8580, Japan (e-mail: hada@esst.kyushu-u.ac.jp).

I. Funaki is with the Institute of Space and Astronautical Science, Japan Aerospace Exploration Agency, Kanagawa 229-8510, Japan (e-mail: funaki@isas.jaxa.jp).

K. P. Shamrai, deceased, was with the Institute for Nuclear Research, National Academy of Sciences of Ukraine, Kiev 03680, Ukraine (e-mail: kshamrai@kinr.kiev.ua).
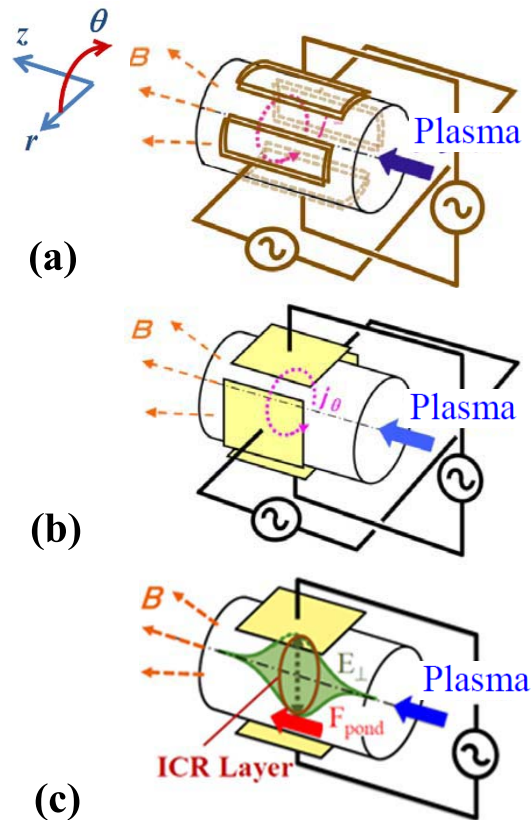
Fig. 1. Proposed electrodeless acceleration schemes. (a) RMF acceleration. (b) REF acceleration. (c) PA with ICR acceleration.

industrial and propulsion applications, along with the particle production efficiency.

We discuss the applicability of our helicon sources with new electrodeless acceleration schemes. Although electric propulsion systems can strongly exceed the chemical systems in their specific impulse (the ratio between exhaust velocity to the gravitational acceleration), many of the conventional electric thrusters [6]–[9] suffer from the problem of finite lifetime caused by the erosion of the electrodes. To avoid this problem, which is the most critical for deep space exploration missions, the completely electrodeless advanced-concept electric thrusters are being developed within the helicon electrodeless advanced thruster (HEAT) project [3]–[5].

We present an overview on our studies on electrodeless plasma thrusters, and discuss the experimental and theoretical approaches on the development of HP-based acceleration schemes including: 1) rotating magnetic field (RMF) acceleration [Fig. 1(a)], which is similar to the field reversed
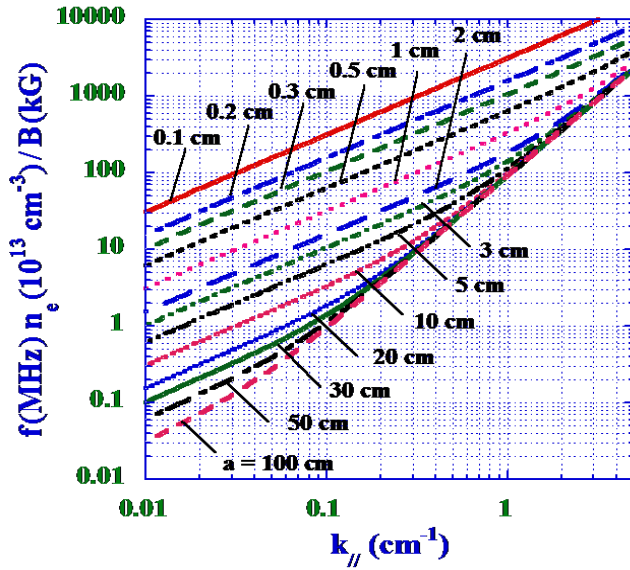
Fig. 2.   Dispersion relation of helicon waves.

Fig. 3.   Electron density n_e as a function of the RF input power P_{inp}, changing the magnetic field near the antenna B_a. The coil current near the antenna equals $I_c = 20, 40, 60$, and 80 A in the cases of red open circles, blue open boxes, green closed diamonds, and black open triangles, respectively.

configuration concept that had been verified in the field of nuclear fusion [10]; 2) rotating electric field (REF) or a Lissajous acceleration [3]–[5], [11] [Fig. 1(b)]; and 3) ponderomotive acceleration (PA) with ion cyclotron resonance (ICR) acceleration [Fig. 1(c)] [4], [5]. Thrust measurements with the high-density helicon sources alone are also presented.

II. HIGH-DENSITY HPs

In this section, the general featured characteristics of the various helicon sources, such as the dispersion relation, mode changes, and production efficiency, are described. In the advanced production scheme, a selective helicon wave excitation of the azimuthal mode is introduced, using a new type antenna called a segmented multiloop antenna.

A. General Featured Characteristics

We examine eight high-density HP sources with different dimensions that operate under a wide range of the magnetic field up to several kilogauss, see [3], [5], [12], and [13]. Fig. 2 is a modification of [2, Fig. 4], which shows the dispersion relation of the helicon waves for a wide variety of plasma radii (a), derived under the assumption of a uniform electron density profile, using the formula from [14]. Here, f, B, and $k_{//}$ are the excitation frequency, the axial component of the static magnetic field, and the parallel wavenumber, respectively. For a plasma with a small diameter, the higher magnetic field is necessary so that the electrons do not to hit the inner wall of the chamber. With an increase in $k_{//}$ (or a decrease in a), the ordinate (the ratio of f n_e/B, where n_e is the plasma density) increases. If n_e and $k_{//}$ are kept constant, the increase in f (or the decrease in B) occurs when a is small.

These results enable to predict the scaling of the plasma radius for the experiments when small or large plasma dimensions are used, as described later. An example of the experimental results, which supplement the data reported in [3],
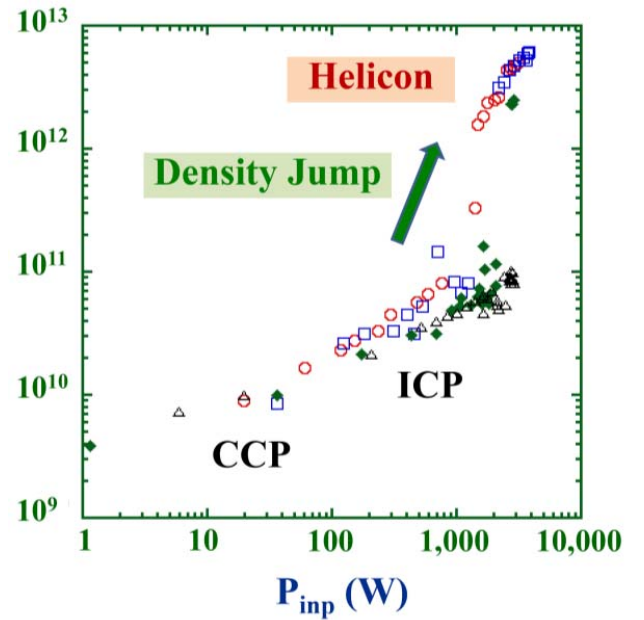
is shown in Fig. 3. This figure shows the dependence of n_e on the radio frequency (RF) input power P_{inp} measured using the developed large helicon plasma device (LHPD) [15] at the Institute of Space and Astronautical Science/Japan Aerospace eXploration Agency with an axial plasma length L_p of 81 cm. The inner diameter (i.d.) of the machine and the axial length are 74 and 486 cm, respectively. A spiral antenna was used for the large diameter plasma production.

With an increase in P_{inp}, n_e increased, and the discharge mode changed from being a capacitively coupled plasma to a HP through an inductively coupled plasma (ICP). When the static magnetic field (axial component) near the antenna B_a was increased, which was controlled by the current in the coil I_c located near this region, the minimum P_{inp} required for a jump in the ICP-to-HP density increased. Here, B_a values were ∼50, ∼90, ∼128, and ∼165 G for $I_c = 20, 40, 60$, and 80 A, respectively. The field away from the antenna was nearly uniform with ∼140 G.

When an axially long and radially narrow HP was operated in a weak magnetic field, the radial classical diffusion was dominated compared with the axial diffusion. The N_e/P_{inp} ratio was expected to be proportional to a^2, where N_e is an overall number of electrons in the plasma [16]. This scaling gives a theoretical upper limit of plasma production, held good in our experiments [3], [5] for a variety of the plasma radii, from the largest source LHPD that was 74 cm in diameter (plasma volume was up to 2.1 m³) [15] to the smallest source that was 2.5 cm in diameter, whose length L_p could be shortened to 4.7 cm (plasma volume was 23 cm³) [17]. Recently, we demonstrated the production of high-density plasma with the plasma radius down to 1.0, 0.5, and 0.25 cm, using the small helicon device (SHD) [5], [18], [19] shown in Fig. 4.
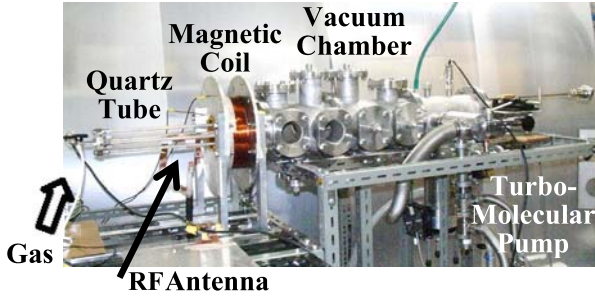
Fig. 4. Photo of SHD.

The axial plasma length L_p is an important parameter regardless of plasma sources. We succeeded in the production of a high-density plasma in the LHPD, where the L_p was changed using various types of termination plates. Plasmas with densities close to 10^{13} and 10^{12} cm^{-3} were produced, respectively, for the longest (L_p = 486 cm) and shortest (L_p = 5.5 cm) plasma lengths, with P_{inp} < 4 kW. The axially short, radially large plasma operated at a quite strong magnetic field. The axial plasma transport dominates, contrary to the previous situation of the dominant radial transport. The N_e/P_{inp} ratio was expected to be proportional to L_p [16], which agreed well with the experimental data.

B. Selective Excitation of the Azimuthal Mode

In addition to the advanced antenna system, we also examined selective excitation of the waves with various azimuthal mode numbers m [14], using a Tokai helicon device (THD) [20], as shown in Fig. 5. This was originally developed to produce a high-density HP that could be used for a variety of nonlinear wave experiments to simulate the space plasma phenomena. The device is currently used to verify the PA/ICR acceleration mechanism (see below) for the HEAT project. An experimental setup, similar to that in Fig. 1(c), was used as the first trial to test the PA/ICR acceleration scheme, which will be described later. However, because only the near field effect of electrodes was used in this configuration, the plasma density was very low, allowing the external fields to effectively penetrate the plasma. Therefore, the effect of the PA/ICR acceleration was barely observed. To improve the situation, we designed an antenna that excited the localized resonant mode of ion-cyclotron frequency range in a high-density plasma that was immersed in a nonuniform background magnetic field.

The THD was equipped with a specially designed segmented multiloop antenna to excite the helicon waves. It was installed just outside the quartz-glass window at the end of the vacuum chamber, as shown in Fig. 5, and consisted of four concentric loops. Each of three outer loops was divided into four equal segments, and the central loop was divided into two equal segments. By varying the electrical connection between the antenna segments, it was possible to excite, not only the waves with $m = 0$, but also those with $m = \pm 1$ and ± 2. For the $m = 0$ excitation, the transition from the ICP to HP discharges occurred at less than $P_{inp} = 1$ kW; then, a HP of $n_e \sim 10^{13}$ cm^{-3} could be easily obtained at $P_{inp} \geq 2$ kW (Ar gas with $P_{Ar} = 0.2$ Pa fill pressure range).

With the $m = \pm 1$ excitation, however, it was difficult to attain the HP mode. An input power of $\sim$2 kW or higher was necessary. The excited wave structures measured by magnetic probes were consistent with those expected from the theory [14]. Similar to the previous experiments performed with the LHPD [3] (see also Fig. 3), the threshold RF power from the ICP to HP discharges was lower when the magnetic field strength near the antenna was weaker than that of the uniform field region where most of the experiments were carried out.

In summary for this section, from the experiments on various HP sources, high-density plasma production was possible for a wide range of source dimensions and could be controlled by changing the plasma length and using a selected excitation from the azimuthal mode. This makes these sources promising for use in the development of the next generation electrodeless thrusters, as well as for fundamental research and industrial applications.

III. ACCELERATION SCHEMES

We have proposed and examined three acceleration methods by external means, such as the RMF, REF, and PA/ICR schemes, as was mentioned. In these concepts, the acceleration electrodes (and production antennas) are indirect contact with the plasma, leading to a longer lifetime operation because of the reduction in the strong plasma–wall interactions. In these schemes, the axial component of the magnetic field B_z is necessary. In addition, the RMF and REF schemes require the radial component of the magnetic field B_r, because the B_r and the induction of the azimuthal current density j_θ in the two schemes create the axial thrust F_z by the electromagnetic (EM) force, $j_\theta \times B_r$.

A. RMF Scheme

The initial RMF experiments were carried out using the large mirror device (LMD) [21], as shown in Fig. 6. The RMF coils (10 turns) were wound around a quartz glass tube (5-cm i.d. and 50-cm axial length), which was inserted into the vacuum chamber. The HP, generated by a single loop antenna with a 4-cm in bandwidth, was accelerated by the RMF scheme. The RF input power P_{inp} and the excitation frequency f were $\sim$2 kW and 7 MHz (for the plasma production), respectively. The P_{RMF} (RMF power) was <1 kW and f_{RMF} (RMF frequency) was 1 MHz (for the RMF method). The radially movable standard and directional Langmuir probes at the axial position of $z = 15$ cm were used to measure the electron density and the ion flow velocity, respectively. To measure the RMF penetration, which is essential in this RMF scheme [22], a magnetic probe was placed at the center of the RMF coils. Here, P_{Ar} was 0.1 Pa, which is important from a viewpoint of the collision frequency v (the summation of electron-ion and electron-neutral collision frequencies), and the electron temperature T_e is typically $\sim$3 eV.

As was previously mentioned, penetration of the RMF is important. The penetration conditions are determined by the
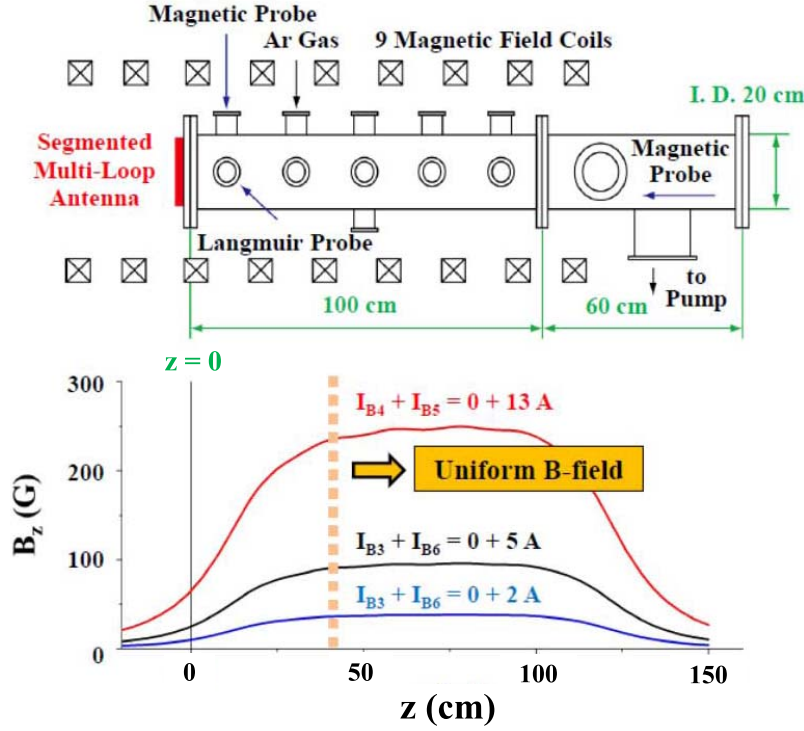
Fig. 5. Schematic diagram and photos of the THD and its segmented multiloop antenna. Three examples of the calculated axial magnetic field profile are also shown. Here, $I_{B4} + I_{B5} = 0 + 13$ A (red curve), where the currents in the first four coils from the far left were 0 A and those in the remaining five coils were 13 A. Likewise, $I_{B3} + I_{B6} = 0 + 5$ A (black curve) or $0 + 2$ A (blue curve), where the currents in the first three coils from the far left were 0 A and those in the remaining six coils were 5 or 2 A.
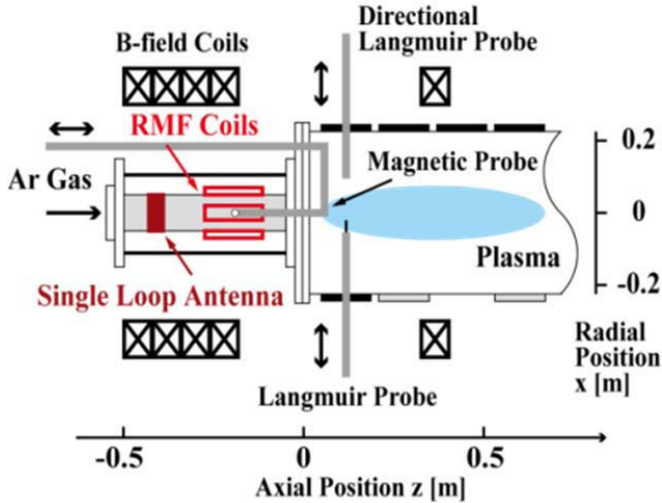

Fig. 6. Experimental setup for the RMF scheme in the LMD.

following two parameters [22]: $\gamma = \omega'_{ce}/\nu$ (the Hall parameter) and $\lambda = a/\delta$ (a reciprocal of the normalized skin depth). Here, ω'_{ce} and δ are an electron cyclotron angular frequency, defined using the RMF strength B_{RMF}, and the skin depth, respectively. To achieve full penetration, a higher value of γ/λ is required, (e.g., >1.12 for $\lambda < 6.5$) [22], showing that a larger B_{RMF} (RMF vertical field) and smaller n_e, f_{RMF}, a, P_{Ar}, and η (plasma resistivity) are necessary. On the other hand, the plasma thrust is proportional to n_e, f_{RMF} (applied RMF frequency), B_r, and a^3 [23] (see the

thrust discussion shown below), which is a tradeoff condition for the above penetration condition. Thus experimentally, we need to compromise between the two conditions of the field penetration and the thrust. In our the initial try, we experimentally confirmed the full field penetration [24] in the expected cases for the partial penetration, in addition to the full penetration from the simulations [22].

Here, we will discuss the thrust in the RMF scheme, whose principle is similar to the thrust coming from the naturally generated electron diamagnetic drift [25] under the presence of a radial pressure gradient. Here, the induced electron current, regardless of the generation mechanism, in the presence of the flaring magnetic field creates the axial component of the EM thrust (causing the electrons and ions to move together because of the ambipolarity). In other words, finally, the axial electric potential formed accelerates the ions.

When there is full penetration of the RMF, the electrons make a rigid rotation. The electron current density is given by: $j_\theta = n_e e r \omega$, where $\omega = 2\pi f_{RMF}$. If the B_r is expressed as: $\sim B_z (r/2R)$ (in the divergent magnetic field region just outside the magnetic field coil with a radius of R) and the electron density is spatially uniform, then the thrust can be estimated as

$$F = L_A \int_0^a j_\theta B_r (2\pi r) dr = \frac{\pi a}{4R} e n_e L_A \omega B_z a^3 \qquad (1)$$

where L_A is the axial length of the accelerating region. For typical values of $\omega = 6 \times 10^6$ s^{-1}, $R \sim a = L_A = 5$ cm, $n_e = 10^{12}$ cm^{-3}, and $B_z = 500$ G, (1) yields $F \sim 100$ mN, which is large enough for the thrust value. We note that
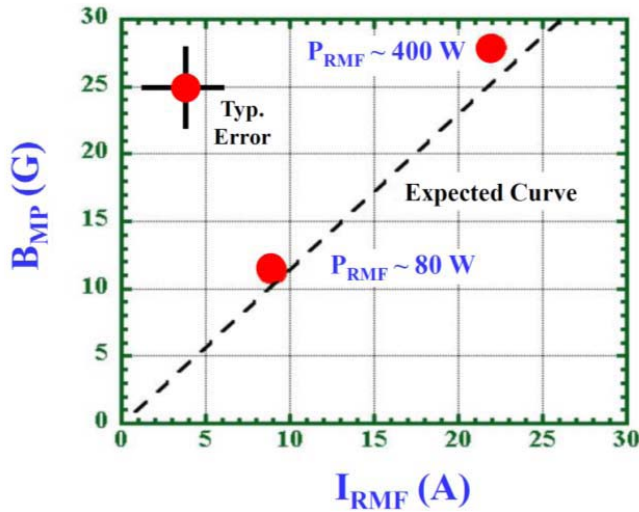
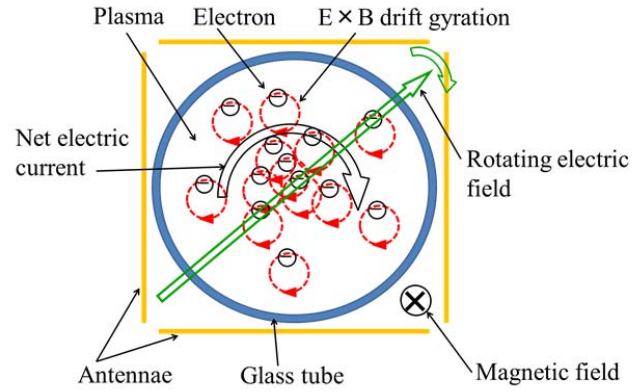Fig. 7. Magnetic probe signal B_{MP} versus the RMF current I_{RMF}.

Fig. 8. Mechanism of the azimuthal electron current that is induced by the REF (cross-sectional plane in the plasma acceleration region of the thruster).

the thrust is not reduced significantly even when the RMF penetration is partial, since the thrust is mainly dominated by the current near the edge of the plasma.

In our experiments, we adjusted the HP performance, which had a high-density up to $\sim 10^{13}$ cm^{-3} in the source region. This was achieved by changing B_z, the magnetic field configuration (the field divergence is important because B_r contributes to the EM force $j_\theta \times B_r$, as was mentioned previously), and P_{Ar}. Especially, by reducing P_{Ar} to have a lower η, it is possible to improve the field penetration condition, bearing in mind that n_e is lower in the acceleration region compared with the source region because of the divergence of the downstream magnetic field.

The initial measurement on the RMF penetration, using a magnetic probe (Fig. 7), showed that the RMF field was in good agreement with the expected curve, using the RMF coil current in the absence of the plasma: $f_{RMF} = 1$ MHz and the RMF current were ~ 9 and 22 A. Radial distributions of the RMF field [5], [24] also supported this measurement. Although there was a slight increase in the flow velocity by this scheme, it was expected from the above-mentioned axial thrust F_z using the EM force $j_\theta \times B_r$, that a higher velocity is necessary to achieve a higher thrust efficiency.

Recently, permanent magnets were installed around the plasma source region, leading to a larger radial component of the magnetic field to increase the thrust in this scheme. It was also expected that the combined use of electromagnets and permanent magnets made the operation of the magnetic field configuration more flexible. A high-density plasma ($\sim 10^{13}$ cm^{-3}) was achieved near the source region in this combined operation.

A theoretical approach for RMF was also used to describe the thrust, using the two important dimensionless parameters: the normalized plasma radius and the resistivity governed electron Hall parameter. For further studies, the role of the following processes need to be specified using fluid or kinetic plasma modeling: 1) the RMF penetration and the induced azimuthal current channel; 2) the spin-up time scale for

the plasma rotation; 3) the electron axial flow and electron transit time normalized by $1/f_{RMF}$; 4) plasma acceleration via the electron current in the divergent field; and 5) plasma detachment.

B. REF Scheme

In the REF plasma acceleration concept, a directional REF was applied to the plasma, using two sets of opposite facing electrodes [17], as shown in Fig. 8. Because the REF vector generates a Lissajous pattern in the cross-sectional plane, this plasma acceleration concept was called the Lissajous plasma acceleration. Fig. 8 shows the mechanism of the azimuthal electron current induction by the REF. When an oscillating voltage is applied to the above-mentioned electrodes, a REF is penetrated in the plasma. In the presence of the axial magnetic field, the cross-sectional trajectory of the electron is produced by the superposition of two gyration motions. One is the Larmor gyration motion, and the other was a gyration motion caused by the $\mathbf{E} \times \mathbf{B}$ drift motion (the Larmor motion is not shown in Fig. 8 because the Larmor radius is much smaller than that of the $\mathbf{E} \times \mathbf{B}$ drift). The rotating frequency of the REF is chosen to be higher than the ion cyclotron frequency but lower than the electron cyclotron frequency. Therefore, electrons (ions) can (cannot) follow the REF. The superposition of the $\mathbf{E} \times \mathbf{B}$ drift gyration motion of all electrons results into the azimuthal electron currents, as shown in Fig. 8. Note that, in this concept, radial density gradients are necessary to generate these currents, and conveniently, the HP has its typical gradient.

Our theoretical and numerical thrust calculations [11], [26]–[28], with the use of the particle-in-cell simulation, where a collisionless plasma was assumed, showed that the ratio of the $\mathbf{E} \times \mathbf{B}$ drift gyration radius of electrons to the plasma diameter was one of the important parameters for the production of the thrust. The maximum thrust was expected to be obtained for a ratio of ~ 0.4. In addition, the range of parameters required for efficient penetration of the REF into plasma was also important, which was estimated. Experimental verification studies were also conducted. Our device had a source glass tube (i.d. 2.6 or 4.6 cm), a magnetic circuit (made of an EM coil or samarium-cobalt permanent magnets,
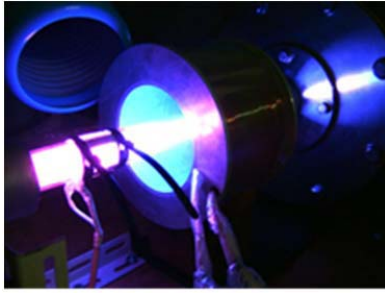
Fig. 9. Operation of the thruster laboratory model using a helicon source (a saddle type antenna is on the left-hand side and a magnetic field coil is in the middle).
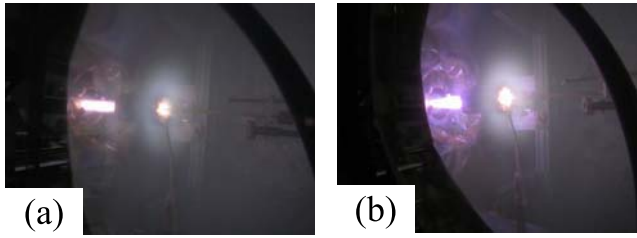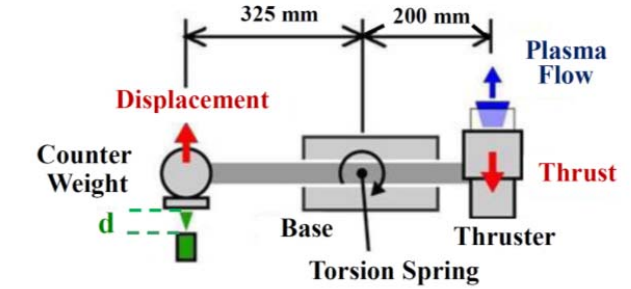

Fig. 10. Plasma light (left-hand side, the bright region was generated in the quartz tube) for the EM thrust force measured in the vacuum chamber (the Ar mass flow rate was 0.4 mg/s). Plasma production for RF powers of (a) 250 and (b) 400 W, which were measured before and after the density jump, respectively.

Fig. 11. Schematic view of the thrust stand of (a) top- and (b) side-view. (c) Photo of the thrust stand.
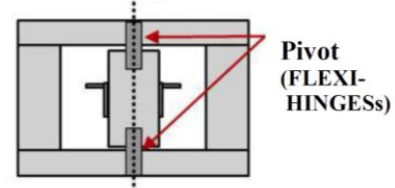
respectively), and RF antennas. In this device, strong blue light emission was observed (Fig. 9), which is the characteristic of HP discharge.

The plasma plume was measured by a para-perp type Mach probe. The flow velocity was increased [5] by applying a REF power input using the following parameters: argon gas with a mass flow rate of 0.1 mg/s, the magnetic field at the Lissajous acceleration region was 950 G, the plasma production power was 300 W with 27.12 MHz, and the REF was applied using the two sets of opposite facing electrodes that was mentioned above (the RF power was 450 W with a frequency of 13.56 MHz, and the antenna voltage applied was 1.4 kV$_{pp}$). However, as to the flow velocity increased, we need to distinguish between the EM and thermal effects, where the latter means that the plasma was heated by the REF and the increment of the thermal energy resulted into an enhancement thrust.
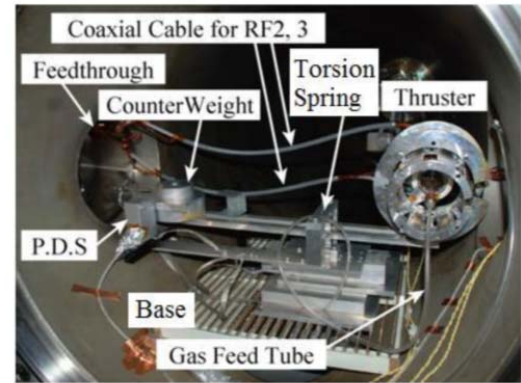
The thrust measurement is essential for the estimation of thrust performance. We also initiated direct measurement of the EM thrust using a torsion pendulum type thrust stand. There was a jump in this EM thrust (from <50 μN to 150–260 μN, depending on conditions), which was associated with a density jump of the plasma [from $\sim 5 \times 10^{16}$ m^{-3} to $(2$–$10) \times 10^{17}$ m^{-3} near the antenna region], which was considered as a helicon mode jump from the ICP to the HP modes. This was successfully observed because the plasma production power became larger than the threshold RF power (~ 250 W in our device): Fig. 10(a) and (b) shows photographs of the plasma light in the thrust measurements before and after the density jump, respectively.

Using HP sources with i.d.s of 5 and 10 cm with permanent magnets installed inside the LHPD device, measurements of the total thrust by also a torsion pendulum type thrust stand and without acceleration methods were performed. Fig. 11 shows an example of this experiment with a source diameter of 5 cm. The abbreviation of P.D.S. is the photo displacement sensor, and the distance d was measured using the P.D.S. To reduce the magnetic coupling to the facility, stainless steel (SUS314) was employed as the chamber material, which was covered by a Mylar sheet to prevent any electric interactions. With this configuration, beam currents were prevented from flowing into the chamber. Because the nonuniform pressure distribution was encountered in this configuration, the pressure value was evaluated near the thruster head.

The recent results that used a larger size (10-cm i.d.) showed the following maximum values by changing the mass flow rate (15–70 sccm) and the input RF power less than 2 kW. A thrust of 11 $\pm$ 0.8 mN, a specific impulse of 840 $\pm$ 60 s, and a thrust efficiency of 2 $\pm$ 0.14% were measured, where shot-to-shot deviations in the thrust value were the most significant source of error.
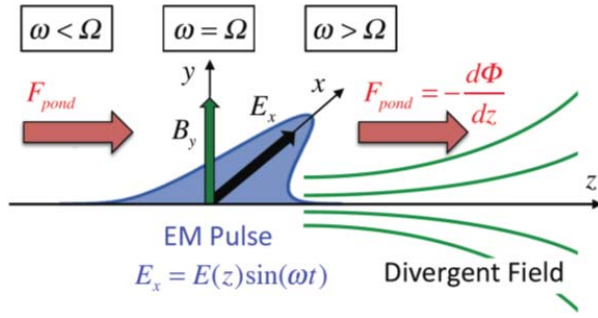
Fig. 12. Concept of the PA/ICR scheme.

Fig. 13. Numerically computed evolution of the parallel and perpendicular energies, $\varepsilon_{//}$ and $\varepsilon_\perp$, of the ions. A typical ion that goes through the region of the RF EM field. The black solid and the red dotted lines correspond to initial ion axial velocities, at its outset at $z = 0$, $v_b = 400$ and 1600 m/s, respectively [33].

Fig. 14. Increment of the ion energy $\Delta\varepsilon$ as a function of the initial axial ion velocity v_b, with a changing width of the RF pulsewidth L_E along with the theoretical line.

C. PA/ICR Scheme

Here, we will discuss the PA/ICR method [Figs. 1(c) and 12]. In this scheme, the ions can be efficiently heated perpendicularly by ICR. In the divergent field, as the ions travel into a region with a weaker magnetic field, their perpendicular energy can naturally be converted into a parallel energy, producing the thrust [29]. In addition, by applying the RF waves in such a way that the resonance point coincides with the peak of the wave energy density, the ions can gain parallel acceleration because of the EM ponderomotive force [30], [31].

The PA and the ICR are inseparable, but the former is preferred because it is less likely to be influenced by the ion–wall interaction caused by the smaller gyroradius. The thrust in this scheme was formulated with ions crossing the region of the ponderomotive potential [31].

$$\phi(z) = \frac{q^2}{4m} \frac{E(z)^2}{\omega^2 - \Omega(z)^2} \tag{2}$$

where q is the ion charge, m is the ion mass, and ω and Ω are the applied angular frequency of the electric field and ion cyclotron angular frequency, respectively. $E(z)$ is the magnitude of the externally applied RF electric field, expressed as follows:

$$\mathbf{E}_{\mathrm{RF}}(z, t) = E(z) \sin(\omega t)\hat{\mathbf{x}}$$
$$E(z) = E_0 \exp\left[-(z - z_{\mathrm{res}})^2/L_E^2\right]. \tag{3}$$

In the above, z_{res} is the location, where $\omega = \Omega(z)$, L_E is the pulsewidth, which refers to the spatial scale at the region of the externally given RF electric field, and $\hat{\mathbf{x}}$ is the unit vector along the x-direction. The magnetic field is the superposition of the RF magnetic field, which is consistent with the above electric field and the background dc field.

$$\mathbf{B}_0 = \left(-\frac{x}{2}B'(z), -\frac{y}{2}B'(z), B(z)\right)$$
$$B(z) = B_0(1 + \tanh[-(z - z_{\mathrm{res}})/L_B]) \tag{4}$$

where the prime indicates the derivative with respect to z, and L_B refers to the spatial scale for the region of the externally given magnetic field.

We calculated the trajectories of the ions and the change in the energy, using this model with the VOLPAL code [32]. Fig. 13 shows the evolution of the parallel and perpendicular energies for a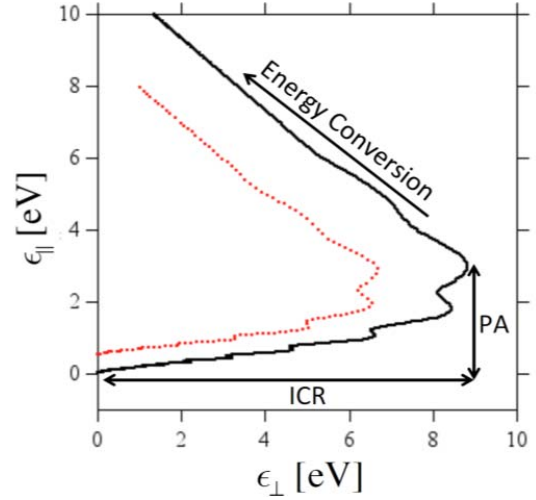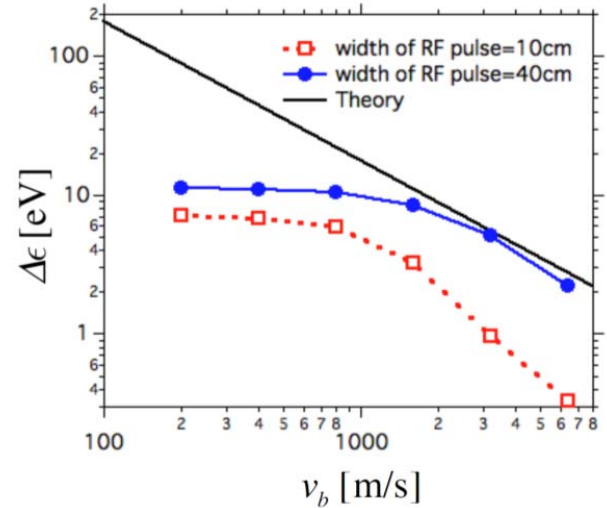 typical ion as it moved through the RF EM field [33]. The red and the blue lines corresponded to the different initial parallel ion velocities of 400 and 1600 m/s, respectively. The acceleration consists of three steps: 1) predominantly perpendicular heating, caused by the ICR, such as the VASIMR project [34]; 2) subsequent parallel acceleration from the PA; and 3) conversion of the perpendicular energy into the parallel energy from the magnetic mirror effect. Initially, the slower particles (black solid line in Fig. 14) stayed within the acceleration region for a longer time and obtained a larger amount of parallel energy eventually, compared with the faster particles (red dotted line in Fig. 13). The contribution of the PA to the final parallel energy gain was about 1/3 of that of the ICR that was under the typical parameters being considered.

The ion energy gain $\Delta\varepsilon$ is plotted against the initial ion parallel velocity at its outset at $z = 0$, labeled as v_b in Fig. 14,
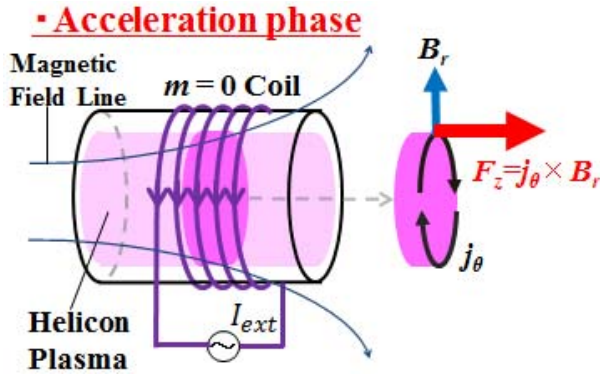
Fig. 15.   Principle of $m = 0$ acceleration, using external coils [24].

Fig. 16.   Conceptual idea of PA using $m = 0$ coils.

for two different values of L_E. The pulsewidth of the RF electric field is defined in (3). In addition, the quasi-linear theory was used to estimate the ICR heating that was caused by the spatially uniform RF field and the nonuniform magnetic field [33]. $\Delta \varepsilon = (\pi q^2 E_0^2 / 4m) (L_B / \omega v_b)$, which is superimposed as a black solid line. When v_b was greater than ~1000 m/s, $\Delta \varepsilon$ decreased as v_b was increased, and the dependence of $\Delta \varepsilon$ on v_b was similar to that predicted by the quasi-linear theory. In particular, when $L_E = 40$ cm (blue solid line), the result from the test particle simulations almost agreed with the quasi-linear estimate, suggesting that the ions stayed within the acceleration region for a long time. Thus, the ICR could operate until the resonance was turned off as the ions moved away from the resonance point. When v_b was less than ~1000 m/s, $\Delta \varepsilon$ appeared to be independent of v_b, because modification of the parallel velocity caused by the ICR and the PA was significant compared with the initial v_b. Recently, we initiated a proof of principle experiment for this scheme using the THD mentioned above. The results were compared with numerical computations that included collisional processes and plasma–wall interactions [35].

D. Other Proposed Schemes

In Section III-A (RMF scheme) and B (REF scheme), we discussed the axial thrust F_z by the EM force, $j_\theta \times B_r$. The essential point here is to induce j_θ by some means with electrodes outside the plasma. One of other methods proposed here is the $m = 0$ acceleration method [3], [24], where the basic idea was to induce again j_θ in the presence of a divergent magnetic field to produce the $j_\theta \times B_r$ axial force, similar to the RMF and REF schemes. Fig. 15 shows the conceptual idea of the acceleration phase, using a low-frequency current applied to the external coil over half of a wave period (in the following half period), a positive (a negative) axial force is expected. The accelerated plasma flow in the negative direction exerts a negative thrust on the spacecraft, leading to a zero net force. If the field driven by the antenna is strong enough to push the plasmoid, during one half-period, out of the acceleration region that was localized just under the antenna, net positive force remains.

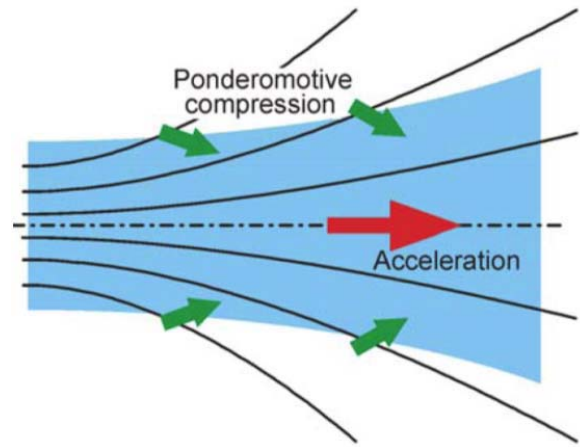The conditions required for the acceleration are follows: 1) the accelerated plasma requires an exhaust from an $m = 0$ antenna area before it undergoes a deceleration phase; 2) the inductance of the plasma is more dominant than the resistance; and 3) the electric and magnetic fields generated by $m = 0$ coil are needed to penetrate the plasma. Thus, the critical operating parameters that were required to achieve an efficient acceleration condition are, an external magnetic field strength, a driving frequency, and the magneto motive force of an $m = 0$ coil.

By improving the computation method [3], the EM fields that are excited by the $m = 0$ antenna were calculated in a 2-D cylindrical geometry. A higher azimuthal current was expected in the range of the ICR frequency. The particle trajectories during one RF period were also estimated to check the plasma motion along the axial direction.

In Section III-C, the ponderomotive force in combination with the ICR was proposed. Another way of to use the ponderomotive force, theoretically, with the $m = 0$ antenna again in a radially nonuniform plasma column is as follows: hybrid modes are formed by coupled helicon and quasi-potential Trivelpiece-Gould waves and have a peripheral localization. These modes have much stronger electric fields than the usual helicon modes, owing to both the presence of the substantial potential component and the effect of nonuniform plasma polarization. For this reason, these modes produce intense ponderomotive effects that are capable of plasma acceleration, even at moderate field amplitudes. This occurs via two mechanisms: direct electron acceleration by the axial force component and plasma compression by a perpendicular force component in a diverging magnetic field, as shown in Fig. 16. The details of this mechanism will be published elsewhere. In the future, test experiment will be carried out to verify the above methods.

IV. CONCLUSION

We presented a review of our recent studies that were performed within the HEAT project, on high-density (~10^{13} cm^{-3}) HP production, and its acceleration schemes. First, a set of featured helicon sources with flexible operation and an ideal, good particle production efficiency were described and characterized to evaluate their potential for use

in applications in a variety of fields. The dimensions of these sources were in the ranges 0.5–74 cm in diameter, and used both the standard $m = 0$ and $m = \pm 1$ helicon antennas, enveloping the discharge volume. The planar side of the antennas, located behind the side dielectric window, included a special segmented antenna for the selective excitation of various azimuthal modes. Second, theoretical and experimental studies on the realization of the proposed acceleration schemes, such as the RMF, REF, and PA/ICR, were discussed from the viewpoint of their application in the development of advanced electrodeless plasma thrusters with enhanced lifetimes. To verify and improve these schemes, further studies are required to extend our understanding on the related physical phenomena and to specify the most appropriate parameter ranges using additional flexible and sophisticated measurements.

In Memoriam

It was a shock, when Shamrai, one of the authors of this paper, suddenly passed away on September 9, 2013. He had taken part in a lot of successful collaborative research around the world. It is a great loss for our community, but his courageous effort in advancing various fields of plasmas science will be remembered for years to come.

Acknowledgment

References

[1] R. W. Boswell, "Plasma production using a standing helicon wave," *Phys. Lett.*, vol. 33A, no. 7, pp. 457–458, Dec. 1970.

[2] S. Shinohara, "Propagating wave characteristics for plasma production in plasma processing field," *Jpn. J. Appl. Phys.*, vol. 36, no. 7B, pp. 4695–4703, Jul. 1997.

[3] S. Shinohara *et al.*, "Development of high-density helicon plasma sources and their applications," *Phys. Plasmas*, vol. 16, no. 5, pp. 057104-1-057104-10, May 2009.

[4] S. Shinohara *et al.*, "Research and development of electrodeless plasma thrusters using high-density helicon sources: The HEAT project," in *Proc. 32th Int. Electr. Propuls. Conf.*, Sep. 2011, pp. 1–10. (Presentation no.: IEPC-2011-056).

[5] S. Shinohara *et al.*, "High-density helicon plasma sources: Basics and application to electrodeless electric propulsion," *Trans. Fusion Sci. Technol.*, vol. 63, no. 1T, pp. 164–167, May 2013.

[6] R. G. Jahn, *Physics of Electric Propulsion*. New York, NY, USA: McGraw-Hill, 1968.

[7] V. G. Grigoryan, "Ion sources for space thrusters (invited)," *Rev. Sci. Instrum.*, vol. 67, no. 3, pp. 1126–1131, Mar. 1996.

[8] C. Charles, "Plasma for spacecraft propulsion," *J. Phys. D, Apply. Phys.*, vol. 42, no. 16, pp. 163001-1–163001-18, Aug. 2009.

[9] E. Ahedo, "Plasmas for space propulsion," *Plasma Phys. Controlled Fusion*, vol. 53, no. 12, pp. 124037-1–124037-18, Dec. 2011.

[10] I. R. Jones, "A review of rotating magnetic field current drive and the operation of the rotamak as a field-reversed configuration (Rotamak-FRC) and a spherical tokamak (Rotamak-ST)," *Phys. Plasmas*, vol. 6, no. 5, pp. 1950–1957, May 1999.

[11] T. Matsuoka *et al.*, "Scaling laws of Lissajous acceleration for electrodeless helicon plasma thruster," *Plasma Fusion Res.*, vol. 6, pp. 2406103-1–2406103-4, Mar. 2011.

[12] S. Shinohara and H. Mizokoshi, "Development of a strong field helicon plasma source," *Rev. Sci. Instrum.*, vol. 77, no. 3, pp. 036108-1–036108-4, Mar. 2006.

[13] S. Shinohara, T. Motomura, K. Tanaka, T. Tanikawa, and K. P. Shamrai, "Large-area high-density helicon plasma sources," *Plasma Sour. Sci. Technol.*, vol. 19, no. 3, pp. 034108-1–034108-10, May 2010.

[14] F. F. Chen, "Plasma ionization by helicon waves," *Plasma Phys. Controlled Fusion*, vol. 3, no. 4, pp. 339–364, Apr. 1991.

[15] S. Shinohara and T. Tanikawa, "Development of very large helicon plasma source," *Rev. Sci. Instrum.*, vol. 75, no. 6, pp. 1941–1946, Jun. 2004.

[16] T. Tanikawa and S. Shinohara. (2004, Oct.). Large-volume, helicon-plasma source for simulation experiments of space plasmas. presented at *Proc. Int. Cong. Plasma Phys.* [Online]. pp. 1–42. Available: http://hal.archivesouvertes.fr/hal-00002013/en/

[17] K. Toki, S. Shinohara, T. Tanikawa, I. Funaki, and K. Shamrai, "Preliminary investigation of helicon plasma source for electric propulsion applications," in *Proc. 28th. IEPC*, Mar. 2003, pp. 1–10. (Presentation no.: IEPC 03-0168).

[18] D. Kuwahara, A. Mishio, T. Nakagawa, and S. Shinohara, "Development of very small-diameter, inductively coupled magnetized plasma device," *Rev. Sci. Instrum.*, vol. 84, no. 8, pp. 103502-1–103502-4, Oct. 2013.

[19] T. Nakagawa, S. Shinohara, D. Kuwahara, A. Mishio, and H. Fujitsuka, "Characteristics of RF-produced, high-density plasma with very small diameter," *JPS Conf. Proc.*, vol. 1, pp. 015022-1–015022-5, Mar. 2014.

[20] T. Tanikawa, S. Shinohara, and T. Motomura, "Research and development of electrodeless plasma rocket engines I. A new helicon-plasma device equipped with a segmented multi-loop antenna," in *Proc. Tokai U., RIST*, vol. 31. Mar. 2012, pp. 4–11.

[21] S. Shinohara, S. Takechi, and Y. Kawai, "Effects of axial magnetic field and Faraday shield on characteristics of RF produced plasma using spiral antenna," *Jpn. J. Appl. Phys.*, vol. 35, no. 8, pp. 4503–4508, Aug. 1996.

[22] R. D. Milroy, "A numerical study of rotating magnetic fields as a current drive for field reversed configurations," *Phys. Plasmas*, vol. 6, no. 7, pp. 2771–2779, Jul. 1999.

[23] M. Inomoto, "Plasma acceleration by using rotating magnetic field," *IEEJ Trans. Fundam. Mater.*, vol. 128, no. 4, pp. 319–320, Nov. 2008.

[24] T. Ishii *et al.*, "Study on electrodeless electric propulsion in high-density helicon plasma with permanent magnets," *JPS Conf. Proc.*, vol. 1, pp. 015047-1–015047-5, Mar. 2014.

[25] K. Takahashi, T. Lafleur, C. Charles, P. Alexander, and R. W. Boswell, "Electron diamagnetic effect on axial force in an expanding plasma: Experiments and theory," *Phys. Rev. Lett.*, vol. 107, no. 23, pp. 235001-1–235001-4, Dec. 2011.

[26] T. Matusoka *et al.*, "One dimensional modeling of radio frequency electric field penetration into magnetized plasmas," *Jpn. J. Appl. Phys.*, vol. 51, no. 9, pp. 096201-1–096201-8, Sep. 2012.

[27] H. Nishida *et al.*, "Study on proof-of-principle of Lissajous acceleration for electrodeless helicon plasma thruster," *Frontier Appl. Plasma Technol.*, vol. 5, no. 2, pp. 67–72, Jul. 2012.

[28] T. Nakamura *et al.*, "Study on helicon plasma Lissajous acceleration for electrodeless electric propulsion," *Trans. JSASS Aerosp. Tech. Jpn.*, vol. 10, no. 28, pp. 17–23, Mar. 2012.

[29] E. A. Bering *et al.*, "Observation of single-pass ion cyclotron heating in a trans-sonic flowing plasma," *Phys. Plasmas*, vol. 17, no. 4, pp. 043509-1–043509-19, Apr. 2010.

[30] I. Y. Dodin, N. J. Fisch, and J. M. Rax, "Ponderomotive barrier as a Maxwell demon," *Phys. Plasmas*, vol. 11, no. 11, pp. 5046–5064, Nov. 2004.

[31] G. Emsellem, "Development of a high power electrodeless thruster," in *Proc. 29th Int. Electr. Propuls. Conf.*, Oct. 2005, pp. 1–9. (Presentation no.: IEPC-2005-156).

[32] *VORPAL, Ver. 4.2*, Tech-X Corporation, Boulder, CO, USA, 2010.

[33] F. Otsuka, T. Hada, S. Shinohara, T. Tanikawa, and T. Matsuoka, "Numerical studies of ponderomotive acceleration and ion cyclotron resonance: Application to next generation electric thrusters," *Plasma Fusion Res.*, vol. 8, pp. 1406012-1–1406012-14, Jan. 2013.

[34] F. R. Chang-Díaz, "The VASIMR rocket," *Sci. Amer.*, vol. 283, pp. 90–97, Nov. 2000.

[35] F. Otsuka, T. Hada, S. Shinohara, T. Tanikawa, and T. Matsuoka, "Numerical modeling of electrodeless electric thruster by ion cyclotron resonance/ponderomotive acceleration," *Plasma Fusion Res.*, vol. 8, pp. 2406067-1–2406067-7, Mar. 2013.

Shunjiro Shinohara received the B.S., M.S., and Ph.D. degrees in physics from the University of Tokyo, Tokyo, Japan, in 1976, 1978, and 1984, respectively.
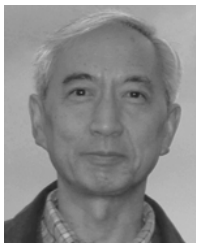
He was an Assistant Professor with the Faculty of Science, University of Tokyo, since 1980, and an Associate Professor with the Interdisciplinary Graduate School of Engineering Sciences, Kyushu University, Fukuoka, Japan. He is currently a Professor with the Institute of Engineering, Tokyo University of Agriculture and Technology, Tokyo. His current research interests include extensive plasma science, including RF discharges (such as helicon discharge), plasma propulsion, nonlinear physics (such as bifurcation, self-organization, and turbulent studies), and the behavior of mangetohydrodynamic in high-temperature plasma/nuclear fusion fields.

Dr. Shinohara was awarded the Commendation for Science and Technology by the Minister of Education, Culture, Sports, Science and Technology, Japan, in 2010.

Tohru Hada received the B.S. degree in geophysics from the University of Tokyo, Tokyo, Japan, and the Ph.D. degree in physics from the University of California, Los Angeles (UCLA), CA, USA, in 1979 and 1985, respectively.

He joined the Faculty of College of General Education, Kyushu University, Fukuoka, Japan, as an Associate Professor in 1989, following post-doctoral work at UCLA. He is currently a Professor with the Interdisciplinary Graduate School of Engineering Sciences, and the Director of the International Center for Space Weather Science and Education, Kyushu University. His current research interests include nonlinear waves and turbulence in space plasma, acceleration of cosmic rays, and theoretical modeling of electric thrusters.

Prof. Hada is a recipient of the Fulbright Fellowship, the UCLA Alumni Association Award for Distinguished Scholars, and the Tanakadate Medal from the Society of Geomagnetism and Earth, Planetary and Space Sciences, Japan.

Hiroyuki Nishida received the B.E. degree in engineering science from Kyoto University, Kyoto, Japan, and the M.E. and Ph.D. degrees in aeronautics and astronautics from the University of Tokyo, Tokyo, Japan, in 2003, 2005, and 2008, respectively.

He was a Post-Doctoral Researcher with the University of Tokyo, Tokyo, Japan, in 2008. Since 2009, he has been an Associate Professor with the Institute of Engineering, Tokyo University of Agriculture and Technology, Tokyo. His current research interests include numerical simulations of fluidic plasma, plasma-assisted flow control techniques, advanced space propulsion systems, and high-angle-of-attack aerodynamics and its control.

Ikkoh Funaki (M'00) received the B.E. degree from the Department of Aeronautics, Kyoto University, Kyoto, Japan, and the M.E. and Ph.D. degrees from the Department of Aeronautics and Astronautics, University of Tokyo, Tokyo, Japan, in 1990, 1992, and 1995, respectively.

He was a part-time Lecturer and then a Research Associate with the Institute of Space and Astronautical Science, Japan Aerospace Exploration Agency, Sagamihara, Japan, from 1995 to 2001, where he was involved in developing microwave discharge ion engines. In 2001, he was a Lecturer with the University of Tsukuba, Tsukuba, Japan. In 2003, he joined the Department of Space Transportation Engineering, Institute of Space and Astronautical Science, Japan Aerospace Exploration Agency, where he is currently an Associate Professor. His current research interests include electric and other advanced spacecraft propulsion systems, plasma application in space, and space plasma physics.

Takao Tanikawa was born in Tokyo, Japan, in 1951. He received the B.S. and M.S. degrees in applied physics from Waseda University, Tokyo, and the Ph.D. degree in physics from the University of California at Los Angeles, Los Angeles, CA, USA, in 1974, 1976, and 1987, respectively.

He was an Associate Professor with the Institute of Research and Development, Tokai University, Tokyo, Japan, from 1988 to 1999. Since 1999, he has been a Professor with the Research Institute of Science and Technology, Tokai University, Kanagawa, Japan. He has been involved in various basic plasma physics experiments related to nonlinear waves, simulation experiments of space plasma phenomena, RF plasma discharge including helicon discharge, plasma propulsion, and active ionospheric experiments.
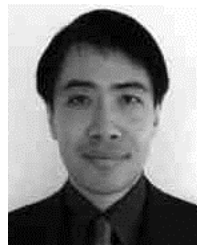
Dr. Tanikawa was awarded the Commendation for Science and Technology by the Minister of Education, Culture, Sports, Science and Technology, Japan, in 2010.

Konstantin P. Shamrai (deceased) passed away on September 9, 2013. He received the B.S. (Diploma) degree in theoretical physics from Kiev State University, Kiev, Ukraine, and the Candidate and Ph.D. degrees in physical and mathematical sciences from Kiev State University and Kharkov National University, Kiev, in 1972, 1976, and 2008, respectively.

He joined the Institute for Nuclear Research, National Academy of Sciences of Ukraine, Kiev, where he was the Head of the Plasma Theory Department. He was also an Invited Professor with Kiev National University. His research interests included the physics of linear, nonlinear and stochastic interactions of electromagnetic waves and charged particle beams with plasmas, physics of helicon plasmas and inductively coupled plasmas, and the applications of high-density plasmas.

Dr. Shamrai was awarded the Commendation for Science and Technology by the Minister of Education, Culture, Sports, Science and Technology, Japan, in 2010.